Instability of the realizable k–ε turbulence model beneath surface waves

Fuhrman, David R.; Li, Yuzhu

Published in:
Physics of Fluids

Link to article, DOI:
10.1063/5.0029206

Publication date:
2020

Document Version
Publisher's PDF, also known as Version of record

Physics of Fluids

Instability of the realizable k–ε turbulence model beneath surface waves

Cite as: Phys. Fluids **32**, 115108 (2020); https://doi.org/10.1063/5.0029206
Submitted: 10 September 2020 . Accepted: 20 October 2020 . Published Online: 04 November 2020

David R. Fuhrman, and Yuzhu Li

Physics of Fluids ARTICLE scitation.org/journal/phf

Instability of the realizable k–ε turbulence model beneath surface waves

Cite as: Phys. Fluids 32, 115108 (2020); doi: 10.1063/5.0029206
Submitted: 10 September 2020 • Accepted: 20 October 2020 •
Published Online: 4 November 2020

David R. Fuhrman[a] and Yuzhu Li[b]

AFFILIATIONS

Department of Mechanical Engineering, Section for Fluid Mechanics, Coastal and Maritime Engineering, Technical University of Denmark, DK-2800 Kgs Lyngby, Denmark

[a]Author to whom correspondence should be addressed: drf@mek.dtu.dk
[b]yuzhuli@mek.dtu.dk

ABSTRACT

Recent research has proved that most widely used two-equation turbulence closure models are unconditionally unstable in regions of nearly potential flow having finite strain, as commonly found beneath non-breaking surface waves. In this work, we extend such analysis to consider the popular realizable k–ε turbulence model. It is proved that this model, unlike all others thus far analyzed, is only conditionally unstable in such regions due to the addition of viscosity in the ε dissipation term. A method for formally stabilizing the model in the problematic regions is likewise developed. The results of the analysis, using both standard and stabilized turbulence closures, are confirmed via numerical simulations of progressive surface wave trains using a computational fluid dynamics model. Important qualitative differences are likewise demonstrated in simulations involving spilling breaking waves. (In the above, k is the turbulent kinetic energy density, and ε is the turbulence dissipation rate.)

I. INTRODUCTION

Recently, Larsen and Fuhrman[1] (hereafter LF18) proved that most widely utilized two-equation turbulence closure models (several variants of both k–ω and k–ε models) are unconditionally unstable in regions of nearly potential flow having finite strain, as commonly found beneath non-breaking surface waves. Their analysis built upon the earlier proof of conditional instability (of the k–ω model) by Mayer and Madsen.[2] These instabilities cause unphysical exponential growth of the turbulent kinetic energy and eddy viscosity and largely explain the widespread, pronounced over-prediction of turbulence in computational fluid dynamics (CFD) studies of surface waves experienced over the past two decades.[1–4]

A popular model that was not analyzed by LF18,[1] however, is the realizable k–ε turbulence model of Shih *et al.*[5] This model is generally more complex than many more traditional two-equation closures for several reasons, including (1) the closure coefficient on the turbulence production term (commonly termed C_μ) not being constant and (2) inclusion of viscosity in the dissipation term in the ε equation.

The present work will fill this gap by systematically analyzing the realizable k–ε model for stability in nearly potential flow regions beneath surface waves. It will be shown that unlike all other two-equation models thus far analyzed, this turbulence model is conditionally (rather than unconditionally) unstable. The range of initial conditions leading to instability will be thoroughly investigated, and a method for stabilizing the model will be developed and confirmed directly through CFD simulations. Clear, qualitative improvement using stabilized variations of the model will be demonstrated for both non-breaking and breaking waves.

II. REALIZABLE k–ε TURBULENCE CLOSURE MODEL

Throughout the present work, we adopt the widely used realizable k–ε model of Shih *et al.*[5] for describing the effects of turbulence on the mean (Reynolds averaged) flow. This model is comprised of transport equations for the turbulent kinetic energy density, $k = 1/2(\overline{u_i' u_i'})$,

$$\frac{\partial(\rho k)}{\partial t} + \overline{u}_j \frac{\partial(\rho k)}{\partial x_j} = \rho P_k - \rho\varepsilon + \frac{\partial}{\partial x_j}\left[\left(\mu + \frac{\mu_{T,0}}{\sigma_k}\right)\frac{\partial k}{\partial x_j}\right] - \rho P_b, \quad (1)$$

as well as the turbulence dissipation rate (per unit mass), ε,

$$\frac{\partial(\rho\varepsilon)}{\partial t} + \overline{u}_j\frac{\partial(\rho\varepsilon)}{\partial x_j} = \rho C_1\sqrt{p_0}\varepsilon - \rho C_2\frac{\varepsilon^2}{k+\sqrt{\nu\varepsilon}} + \frac{\partial}{\partial x_j}\left[\left(\mu + \frac{\mu_{T,0}}{\sigma_\varepsilon}\right)\frac{\partial\varepsilon}{\partial x_j}\right] - \rho C_{1\varepsilon}\frac{\varepsilon}{k}C_{3\varepsilon}P_b. \quad (2)$$

Here, $\overline{u}_j$ are the mean components of the velocity, x_j are the Cartesian coordinates, $\mu = \rho\nu$ is the dynamic molecular viscosity, ν is the kinematic viscosity, $\mu_{T,0} = \rho C_\mu k^2/\varepsilon$, ρ is density, and t is time. The Reynolds stress tensor is defined according to the Boussinesq approximation

$$\frac{\tau_{ij}}{\rho} = -\overline{u_i'u_j'} = 2\nu_T S_{ij} - \frac{2}{3}k\delta_{ij}, \quad (3)$$

where

$$\nu_T = \frac{\mu_T}{\rho} = C_\mu\frac{k^2}{\tilde{\varepsilon}}, \quad (4)$$

$$S_{ij} = \frac{1}{2}\left(\frac{\partial\overline{u}_i}{\partial x_j} + \frac{\partial\overline{u}_j}{\partial x_i}\right). \quad (5)$$

In the above, an overbar signifies time (ensemble) averaging, a prime superscript denotes turbulent (fluctuating) components, δ_{ij} is the Kronecker delta, S_{ij} is the mean strain rate tensor, and ν_T is the kinematic eddy viscosity. For the standard version of the model, $\tilde{\varepsilon} = \varepsilon$ (hence $\mu_T = \mu_{T,0}$), with $\tilde{\varepsilon}$ introduced here for later use. The shear production term for k is

$$P_k = \frac{\tau_{ij}}{\rho}\frac{\partial\overline{u}_i}{\partial x_j} = p_0\nu_T, \quad (6)$$

where

$$p_0 = 2S_{ij}S_{ij}. \quad (7)$$

Similarly, the buoyancy production for k is formulated as

$$P_b = -\frac{g_i}{\rho}\overline{\rho' u_i'} = p_b\nu_T, \quad (8)$$

$$p_b = \frac{1}{Pr}N^2, \quad (9)$$

$$N^2 = \frac{g_i}{\rho}\frac{\partial\rho}{\partial x_i}, \quad (10)$$

where Pr is the Prandtl number, $(g_1, g_2, g_3) = (0, 0, -g)$ is gravitational acceleration, and N is the Brunt–Vaisala frequency. Additional parameters correspond to

$$C_1 = \max\left[0.43, \frac{\eta}{\eta+5}\right], \quad (11)$$

$$\eta = \sqrt{p_0}\frac{k}{\varepsilon}, \quad (12)$$

$$C_\mu = \frac{1}{A_0 + A_s\frac{kU^*}{\varepsilon}}, \quad (13)$$

$$U^* = \sqrt{S_{ij}S_{ij} + \Omega_{ij}\Omega_{ij}}, \quad (14)$$

$$\Omega_{ij} = \frac{1}{2}\left(\frac{\partial\overline{u}_i}{\partial x_j} - \frac{\partial\overline{u}_j}{\partial x_i}\right), \quad (15)$$

$$A_s = \sqrt{6}\cos\phi, \quad (16)$$

$$\phi = \frac{1}{3}\cos^{-1}\left(\sqrt{6}W\right), \quad (17)$$

$$W = \frac{S_{ij}S_{jk}S_{ki}}{\tilde{S}^3}, \quad (18)$$

$$\tilde{S} = \sqrt{S_{ij}S_{ij}}, \quad (19)$$

where a fixed (non-rotating) reference frame is assumed in the formulation of (14). We use the following standard closure coefficients: $A_0 = 4.0$, $C_{1\varepsilon} = 1.44$, $C_2 = 1.9$, $\sigma_k = 1.0$, $\sigma_\varepsilon = 1.2$, $Pr = 0.85$, and $C_{3\varepsilon} = -0.33$. Note also, for later use, that the transition of C_1 from a constant to being dependent on η occurs at $\eta = \eta_{trans} = 3.771\,93$.

III. STABILITY ANALYSIS

A. Simplifying assumptions

Consider a fluid region having constant density ρ beneath a small amplitude plane surface wave train propagating in the pure horizontal x direction. Mayer and Madsen[2] showed that if the velocity field stemming from linear (potential flow) wave theory was substituted into (7), after period averaging, p_0 will be finite throughout the water column. Upon further depth-averaging their result, LF18[1] showed that this (square of the strain-rate magnitude) corresponds to

$$\langle p_0\rangle = \frac{k_w^2H^2\omega_w^2}{2k_wh\tanh(k_wh)}. \quad (20)$$

Here, $\omega_w = 2\pi/T$ is the angular frequency of the wave, T is the wave period, H is the wave height, k_w is the wave number, and h is the water depth. Based on this, following both Mayer and Madsen[2] and LF18,[1] we will therefore consider p_0 fixed for analysis purposes. In the potential flow region beneath surface waves, it can also be shown that $\langle W\rangle = 0$, leading to $\langle A_s\rangle = 3/\sqrt{2} \approx 2.12$, and we will thus likewise adopt these values as fixed in the analysis that follows. Again following Mayer and Madsen[2] and LF18,[1] we will also neglect convective and diffusive terms, which is reasonable in the potential flow region. From the considerations above, the governing partial differential equations (PDEs) (1) and (2) reduce to the following, much simpler, system of nonlinear ordinary differential equations (ODEs):

$$\frac{\partial k}{\partial t} = k'(t) = \frac{C_\mu k^2 p_0}{\tilde{\varepsilon}} - \varepsilon, \quad (21)$$

$$\frac{\partial\varepsilon}{\partial t} = \varepsilon'(t) = C_1\sqrt{p_0}\varepsilon - \frac{C_2\varepsilon^2}{k+\sqrt{\nu\varepsilon}}. \quad (22)$$

These may be equivalently re-formulated as

$$\Gamma_k = \frac{1}{k}\frac{\partial k}{\partial t} = \sqrt{p_0}\left(C_\mu\eta\frac{\varepsilon}{\tilde{\varepsilon}} - \frac{1}{\eta}\right), \quad (23)$$

$$\Gamma_\varepsilon = \frac{1}{\varepsilon}\frac{\partial \varepsilon}{\partial t} = \sqrt{p_0}\left(C_1 - \frac{C_2}{\eta + \gamma}\right), \tag{24}$$

where the two non-dimensional variables η, as defined in (12), and

$$\gamma = \sqrt{\frac{\nu p_0}{\varepsilon}} \tag{25}$$

uniquely define the state at any time t. The simplified nonlinear ODEs (23) and (24) will form the basis for the stability analysis that follows.

B. Analysis of the standard model assuming $\gamma \ll \eta$

Consider first the case where viscosity is negligible in the ε dissipation term, $\gamma \ll \eta$ [equivalently, $\sqrt{\nu\varepsilon} \ll k$ or $k^2/(\nu\varepsilon) \gg 1$]. In this case, the ε equation (22) reduces to

$$\frac{\partial \varepsilon}{\partial t} = \varepsilon'(t) = C_1\sqrt{p_0}\varepsilon - \frac{C_2\varepsilon^2}{k} \tag{26}$$

or equivalently (24) to

$$\Gamma_\varepsilon = \frac{1}{\varepsilon}\frac{\partial \varepsilon}{\partial t} = \sqrt{p_0}\left(C_1 - \frac{C_2}{\eta}\right), \tag{27}$$

whereas the k equation remains as (23), with $\tilde{\varepsilon} = \varepsilon$ (standard model). Following LF18,[1] it is convenient to consider the asymptotic evolution of a utility variable, somehow involving the ratio of k to ε. When analyzing the standard k–ε turbulence closure model, LF18[1] utilized the specific dissipation rate $\omega = \varepsilon/(C_\mu k)$ for this purpose. However, in the realizable k–ε turbulence model, since C_μ is not simply a constant, it is more convenient to utilize the variable η for this purpose. Invoking (23) and (27), the resulting equivalent ODE for η is

$$\frac{1}{\sqrt{p_0}}\frac{\partial \eta}{\partial t} = \frac{k'(t)}{\varepsilon(t)} - \frac{k(t)\varepsilon'(t)}{\varepsilon(t)^2} = C_2 - 1 - \frac{\eta^2}{5+\eta} + \frac{\eta^2}{A_0 + A_s\eta/\sqrt{2}}, \tag{28}$$

where it has been assumed that $\eta > \eta_{trans}$ such that $C_1 = \eta/(5 + \eta)$, which will be shown to asymptotically be the case. From inspection of (28), it is clear that it is de-coupled from other variables and that η will asymptotically evolve to an equilibrium value such that $\partial\eta/\partial t = 0$, regardless of its initial value. To find the asymptotic value η_∞, we set (28) equal to zero, invoke closure coefficients, and then solve for η. This leads to three roots, two of which are complex and hence not physical. The third (and lone physical) root corresponds to the asymptotic value $\eta_\infty \approx 7.898$.

Once η evolves to become effectively constant at $\eta = \eta_\infty$, then $C_1 \approx 0.6123$ and $C_\mu \approx 0.063\,10$ are likewise constant. The governing equations (23) and (27) thus become effectively linearized and are of the form

$$\frac{1}{k}\frac{\partial k}{\partial t} = \frac{1}{\varepsilon}\frac{\partial \varepsilon}{\partial t} = \frac{1}{\nu_T}\frac{\partial \nu_T}{\partial t} = \Gamma_\infty \approx 0.3718\sqrt{p_0}, \tag{29}$$

where Γ_∞ is the asymptotic exponential growth rate. As this is positive, the model at the limit where $\gamma \ll \eta$ (i.e., negligible viscosity in the ε dissipation term) is unconditionally unstable, i.e., k and ε (hence ν_T) will inevitably (asymptotically) grow exponentially.

The analysis of the realizable k–ε model at this limit is similar to that of all of the various two-equation models analyzed by LF18,[1] which also do not include viscosity in the (ε or ω) dissipation terms. Notably, the resulting value for Γ_∞ found above for the realizable k–ε model is significantly larger than for any of the models analyzed by LF18.[1] For completeness and to ease comparison with the results summarized in their Table 1, the above likewise leads to the asymptotic value for the specific dissipation rate of $\omega_\infty \approx 2.006\sqrt{p_0}$. This is lower than any of the widely used two-equation turbulence models analyzed by LF18.[1] Note that we will only consider $\eta \le \eta_\infty$ in what follows since at this threshold, the scales of the turbulence (characterized by ω_∞ immediately above) become similar in magnitude to those of the mean flow (characterized by $\sqrt{p_0}$). Hence, any reasonable initial conditions (denoted k_0, ε_0) should satisfy $\eta_0 = \sqrt{p_0}k_0/\varepsilon_0 \le \eta_\infty$ with this model.

C. Analysis of the standard model assuming $\eta \ll \gamma$

Consider now the special case where viscosity is large, i.e., $\eta \ll \gamma$ [equivalently, $\sqrt{\nu\varepsilon} \gg k$ or $k^2/(\nu\varepsilon) \ll 1$]. In this case, the ε equation (22) reduces to

$$\frac{\partial \varepsilon}{\partial t} = C_1\sqrt{p_0}\varepsilon - \frac{C_2\varepsilon^2}{\sqrt{\nu\varepsilon}}, \tag{30}$$

whereas the k equation again remains as (23), with $\tilde{\varepsilon} = \varepsilon$ (standard model). Assuming C_1 is constant (since η is assumed small), this equation is de-coupled from the k equation. Upon inspection, it will thus asymptotically evolve to a state where $\partial\varepsilon/\partial t = 0$, corresponding to $\varepsilon_\infty = C_1^2 p_0 \nu/C_2^2$. Inserting this value for ε back into the k equation (23) then leads to

$$\Gamma_k = \frac{1}{k}\frac{\partial k}{\partial t} = \sqrt{p_0}\left(\frac{C_2^2 C_\mu \eta}{C_1^2\gamma^2} - \frac{C_1^2\gamma^2}{C_2^2\eta}\right). \tag{31}$$

Since we here assume that $\gamma \gg \eta$, it is then clear that the second (negative) term in the right-hand side will dominate, i.e., that $\Gamma_k < 0$ and k will inevitably be decaying. This thus proves that at the limit where $\eta \ll \gamma$, (in stark contrast to Sec. III B) the resulting model will be stable.

D. Analysis of the standard model including both γ and η

Let us now conduct a stability analysis of the full ODE system comprised of (23) and (24), i.e., retaining both η and γ in the ε dissipation term, the dynamics of which are considerably more complex than in either of the special cases considered above. In this case, again taking $\tilde{\varepsilon} = \varepsilon$ (standard model), the equivalent ODE for η reads

$$\frac{1}{\sqrt{p_0}}\frac{\partial \eta}{\partial t} = \frac{\gamma(C_1\eta - 1 + C_\mu\eta^2) + \eta(C_2 - 1 - C_1\eta + C_\mu\eta^2)}{\gamma + \eta}. \tag{32}$$

Similarly, we find the following equivalent ODE for γ:

$$\frac{1}{\sqrt{p_0}}\frac{\partial \gamma}{\partial t} = -\frac{1}{2}\sqrt{\frac{\nu}{\varepsilon^3}}\varepsilon'(t) = \frac{\gamma(C_2 - C_1(\gamma + \eta))}{2(\gamma + \eta)}. \tag{33}$$

From inspection of (23) and (24), it is clear that eventual instability will require that $\partial\eta/\partial t > 0$ and $\partial\gamma/\partial t < 0$ such that the system will be evolving toward the asymptotic state found in Sec. III B. From (32)

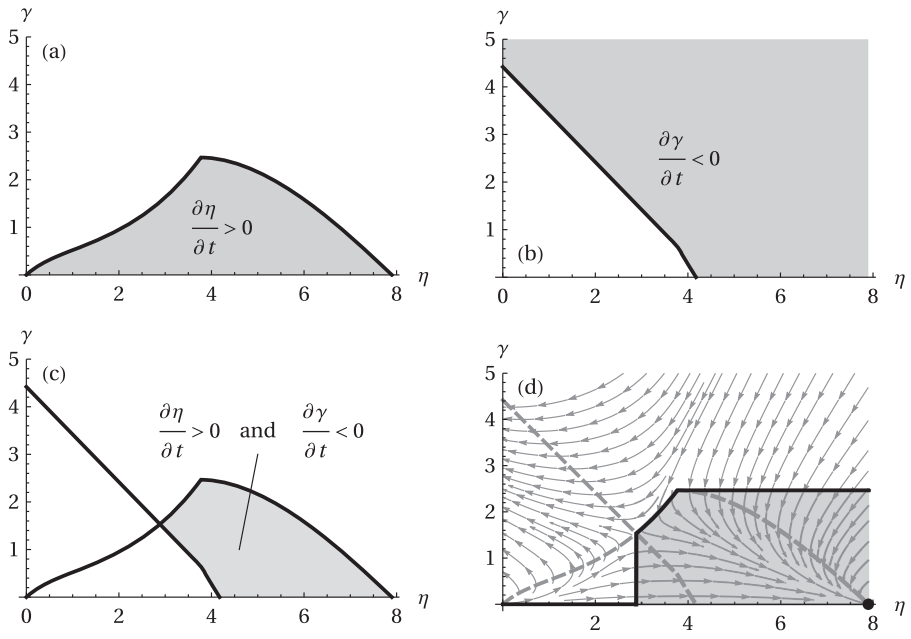

FIG. 1. Regions in the η–γ plane where (a) $\partial\eta/\partial t > 0$, (b) $\partial\gamma/\partial t < 0$, and (c) both $\partial\eta/\partial t > 0$ and $\partial\gamma/\partial t < 0$. In (d), the shaded region represents the "event horizon" region formally proved to inevitably lead to instability, with the point at $(\eta, \gamma) = (7.898, 0)$ representing the asymptote. Streams based on the vector field $1/\sqrt{p_0}(\partial\eta/\partial t, \partial\gamma/\partial t)$ are also shown in (d).

and (33), we, respectively, find that these constraints correspond to the following regions:

$$\frac{\partial \eta}{\partial t} > 0: \qquad \gamma < \frac{\eta(C_2 - 1 - C_1\eta + C_\mu\eta^2)}{1 + C_1\eta - C_\mu\eta^2}, \tag{34}$$

$$\frac{\partial \gamma}{\partial t} < 0: \qquad \gamma > \frac{C_2}{C_1} - \eta. \tag{35}$$

These regions are, respectively, plotted in the η–γ plane in Figs. 1(a) and 1(b), and their intersection is plotted in Fig. 1(c). To gain further insight, a stream plot based on the vector field $1/\sqrt{p_0}(\partial\eta/\partial t, \partial\gamma/\partial t)$, utilizing (32) and (33), is additionally plotted in Fig. 1(d). From this plot, it is clear that (based only on knowledge of the sign of $\partial\eta/\partial t$ and $\partial\gamma/\partial t$) if the solution ever evolves into the shaded region in Fig. 1(d) (henceforth called the formally proved "event horizon," to make a cosmic analogy), corresponding to

$$\gamma \le \begin{cases} 0, & \eta \le \eta_{thresh} = 2.886 \\ \frac{\eta(C_2 - 1 - C_1\eta + C_\mu\eta^2)}{1 + C_1\eta - C_\mu\eta^2}, & \eta_{thresh} < \eta \le \eta_{trans} = 3.772 \\ 2.466\,53, & \eta_{trans} < \eta \le \eta_\infty = 7.898, \end{cases} \tag{36}$$

then it will inevitably (asymptotically) evolve to the point $(\eta, \gamma) = (\eta_\infty \approx 7.898, 0)$ (akin to a "black hole," maintaining the cosmic analogy above). This point corresponds precisely to the asymptotic state predicted at the $\gamma \ll \eta$ limit from Sec. III B and is depicted as the filled circle in the lower right of Fig. 1(d). The above thus proves that the realizable k–ε model (now retaining both γ and η in the ε dissipation term) is conditionally unstable in a potential flow region having finite strain. This is in contrast to all of the two-equation turbulence closure models analyzed by LF18,[1] which were proved to be unconditionally unstable, under the same simplifying assumptions as made here.

The stream plot in Fig. 1(d), however, suggests that the full range of initial conditions (η_0, γ_0), which will asymptotically lead to instability lie well outside the formally proved "event horizon" [shaded region in Fig. 1(d)]. While we have not managed to formally (analytically) prove the exact range of asymptotically unstable initial conditions, owing to the nonlinearity of the governing ODEs, this range is easy to determine numerically. To investigate this in detail, we have therefore performed numerical solutions to (23) and (24) where the initial conditions in terms of (η_0, γ_0) have been systematically varied. This results in the unstable region of initial conditions

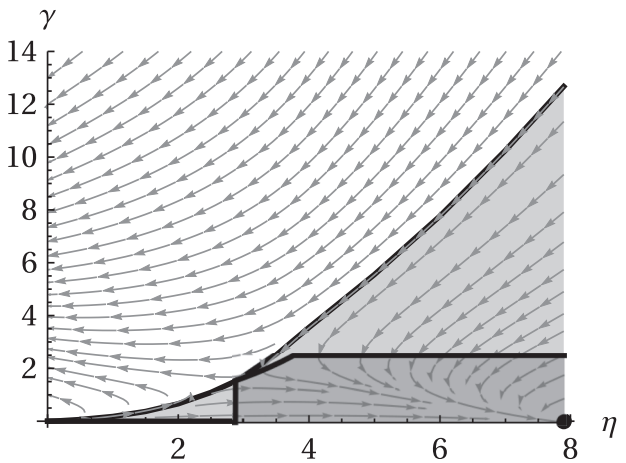

FIG. 2. Light shaded region: Range of initial conditions leading to instability based on the numerical solutions of (23) and (24). Dark shaded region: Formally proved "event horizon" region inevitably leading to instability with the asymptote at $(\eta, \gamma) = (7.898, 0)$. Streams based on the vector field $1/\sqrt{p_0}(\partial\eta/\partial t, \partial\gamma/\partial t)$ are also shown.

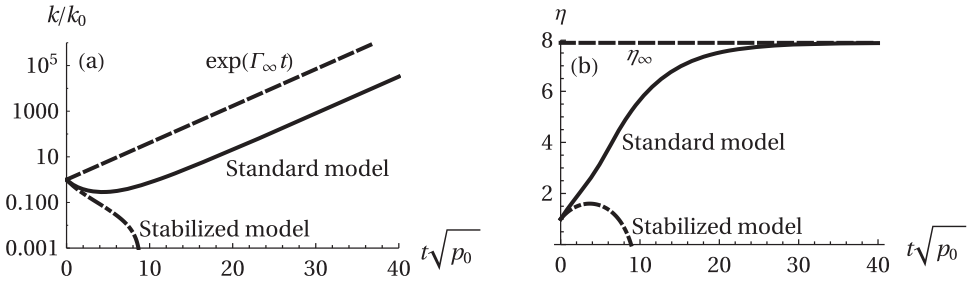

FIG. 3. Example results depicting (a) k/k_0 and (b) $\eta = \sqrt{p_0}k/\varepsilon$ from numerical simulations using standard (full lines) and stabilized (dashed-dotted lines) models based on (23) and (24), with initial conditions corresponding to $(\eta_0, \gamma_0) = (1, 0.1)$. The dashed line in (a) depicts exponential growth at the predicted asymptotic rate Γ_∞ from (29), whereas in (b), it depicts the predicted asymptotic value $\eta = \eta_\infty = 7.8903$. Stabilized model results use $p_\Omega/p_0 = 0.03$ with $\lambda_2 = 0.05$.

depicted in Fig. 2. The formally proved "event horizon" is likewise shown (darker shaded region) and is seen to be a sub-set of the full unstable region, as expected. The stream plot is likewise also depicted on this figure, and the numerically found range of unstable initial conditions corresponds closely to expectations based on these vector streams. Some typical example results from an unstable numerical simulation are depicted in Fig. 3 (full lines), here using initial conditions $(\eta_0, \gamma_0) = (1, 0.1)$. As seen, η quickly approaches its asymptotic value $\eta_\infty = 7.898$ [dashed line in Fig. 3(b)], and once this is reached, k grows exponentially at the rate predicted by (29) [dashed line in Fig. 3(a)].

E. Analysis of a new and formally stabilized model

We will now devise a new version of the realizable k–ε turbulence model that will remove the conditional instability identified above in a region of nearly potential flow having finite strain, again as commonly found beneath non-breaking surface waves. As it has been shown above that when unstable, the model will ultimately evolve to the point $(\eta, \gamma) = (\eta_\infty \approx 7.898, 0)$, it is sufficient for this purpose to specifically stabilize the "worst case" scenario, i.e., where $\gamma = 0$. Similar to several turbulence closure models analyzed by LF18,[1] it turns out that the realizable k–ε model can be stabilized by a simple modification to the eddy viscosity ν_T. This may be accomplished by taking ν_T as defined in (4), but now with

$$\tilde{\varepsilon} = \max\left(\varepsilon, \lambda_2 A \frac{p_0}{p_\Omega}\varepsilon\right), \tag{37}$$

where

$$p_\Omega = 2\Omega_{ij}\Omega_{ij} \tag{38}$$

is analogous to p_0 from (7), but in terms of the rotation-rate tensor,

$$\Omega_{ij} = \frac{1}{2}\left(\frac{\partial \overline{u}_i}{\partial x_j} - \frac{\partial \overline{u}_j}{\partial x_i}\right), \tag{39}$$

and $A = O(1)$ is a constant to be determined such that the physical meaning of $\lambda_2 \ll 1$ (an added stress limiter coefficient) will be clear, and analogous to that defined for several other models by LF18.[1] By design, it is seen that the new limiter [second argument in (37)] will only become active in a nearly potential flow region having finite strain, i.e., where $p_\Omega \ll p_0$, corresponding precisely to the conditions where the model has been proved to be conditionally unstable. Conversely, in sheared regions of primary interest, p_0 and p_Ω will be of the same order of magnitude such that the first argument in (37) will dominate, and the model reverts naturally to its standard form.

Consider now a nearly potential flow region having finite strain such that the second argument in (37) dominates. The k equation (21) then becomes

$$\frac{\partial k}{\partial t} = \frac{C_\mu k^2 p_\Omega}{A\lambda_2 \varepsilon} - \varepsilon \tag{40}$$

or, equivalently, (23) becomes

$$\Gamma_k = \frac{1}{k}\frac{\partial k}{\partial t} = \sqrt{p_0}\left(\frac{C_\mu \eta p_\Omega}{A\lambda_2 p_0} - \frac{1}{\eta}\right), \tag{41}$$

whereas the ε equation, under present assumptions, remains equivalent to (27). In this case, the resulting equivalent equation for η works out to be

$$\frac{1}{\sqrt{p_0}}\frac{\partial \eta}{\partial t} = C_2 - 1 - C_1\eta + C_\mu \eta^2 \frac{p_\Omega}{p_0 A\lambda_2}. \tag{42}$$

Let us first assume that $\eta > \eta_{trans}$ such that $C_1 = \eta/(\eta + 5)$. We may then insert this, and also C_μ from (15), into (42). Setting the result equal to zero, we may then solve for $\eta = \eta_\infty$, resulting in three roots, each of which is rather complicated. To keep the analysis tractable, we insert closure coefficients and Taylor expand the lone physical (positive) root about $p_\Omega/p_0 = 0$, leading to the following much simpler expression:

$$\eta_\infty = 2.6185 + \frac{1.5193}{A\lambda_2}\frac{p_\Omega}{p_0} + O\left(\frac{p_\Omega}{p_0}\right)^2. \tag{43}$$

Invoking this result within (41) then leads to a rather complicated expression for the asymptotic growth rate Γ_∞ defined in (29). Again, Taylor series expanding the result about p_Ω/p_0 to keep it tractable yields

$$\Gamma_\infty \approx \sqrt{p_0}\left(-0.3819 + \frac{0.5519 p_\Omega}{A\lambda_2 p_0}\right). \tag{44}$$

Thus, to leading order in p_Ω/p_0, the resulting model will be stable (i.e., $\Gamma_\infty \le 0$) where

$$\frac{p_\Omega}{p_0} \le 0.6920\, A\lambda_2 \qquad \text{or} \qquad \frac{p_\Omega}{p_0} \le \lambda_2, \qquad A = 1.445. \tag{45}$$

In the above, A has been chosen such that the stress-limiter λ_2 defines the threshold for stability in terms of p_Ω/p_0 in the same fashion as in LF18.[1]

For completeness, it is also necessary to check the case where $\eta \le \eta_{trans}$ such that $C_1 = 0.43$. In this case, following the steps described just above, while also invoking the value for A above, leads to

$$\eta_\infty = 2.0930 + \frac{0.9874}{\lambda_2}\frac{p_\Omega}{p_0} + O\left(\frac{p_\Omega}{p_0}\right)^2 \tag{46}$$

and

$$\Gamma_\infty \approx \sqrt{p_0}\left(-0.4778 + \frac{0.4283 p_\Omega}{\lambda_2 p_0}\right). \tag{47}$$

Thus, in this case, the model will be formally stable where $p_\Omega/p_0 \le 1.116\lambda_2$. As this range (slightly) exceeds that in (45), the value for A given above is conservative.

To conclude, simply switching to an eddy viscosity defined in (4), but with $\tilde{\varepsilon}$ now defined according to (37), results in a new version of the realizable k–ε model that is formally stable in regions of the nearly potential flow region having finite strain, as defined by (45). Stability has been confirmed via numerous numerical simulations of (23) and (24), an example of which can be seen in Fig. 3 (dashed-dotted lines).

IV. TESTING WITH A CFD MODEL

We will now test the analysis-based predictions regarding the stability of the realizable k–ε model directly through CFD simulations. For this purpose, we utilize the same CFD model in the open-source software OpenFOAM as in LF18,[1] wherein the full model equations defined in Sec. II are utilized to close a two-phase (water–air) model solving Reynolds-averaged Navier–Stokes equations[1] (and references therein).

A. Wave train simulations

As an initial test, we consider simulations involving propagation of a theoretically steady wave train having period $T = 2$ s and wave height $H = 0.125$ m on a water depth $h = 0.4$ m ($k_w H = 0.207$, $k_w h = 0.664$), based on the solution of Fenton[6] as implemented by Jacobsen *et al.*[7] Except for the turbulence model (and variety of initial conditions k_0 and ε_0), the setup is otherwise identical to that described in detail in LF18,[1] making use of periodic lateral boundaries. Note that for the present conditions, (20) yields $\langle p_0 \rangle = 0.55$, and this fixed value for p_0 will be utilized for comparison with the analysis in what follows.

For testing purposes, we have systematically varied the initial conditions in terms of (η_0, γ_0) using both standard ($\lambda_2 = 0$ such that $\tilde{\varepsilon} = \varepsilon$) and stabilized ($\lambda_2 = 0.05 \ll 1$) versions of the full realizable k–ε turbulence model. The results are summarized in Fig. 4. In this figure, filled circles indicate initial conditions leading to instability (exponential growth) of the turbulent kinetic energy and eddy viscosity, whereas open circles indicate those that did not. The results from the standard realizable k–ε model, Fig. 4(a), generally confirm that this model is indeed conditionally unstable. The range of initial conditions leading to instability generally (though not perfectly) follows the tendencies predicted from our analysis based on the simplified system of ODEs (23) and (24), shown as the shaded region. The minor discrepancies are not altogether surprising, given that the analysis (for reasons of simplicity) has assumed constant p_0, whereas in the full CFD, this parameter varies in two spatial dimensions and in time. The simplified analysis likewise has neglected several (convective, diffusive, and also buoyancy production) terms that are included in the CFD model. Despite these differences, the simplified analysis seems to have convincingly diagnosed the fundamental reasons for this problem.

Testing with the stabilized model, Fig. 4(b), likewise confirms that the model is stabilized by simply switching to $\tilde{\varepsilon}$ defined in (37). This is again consistent with our simplified analysis of this problem in Sec. III E. As an example demonstrating the qualitative differences, the results from otherwise identical simulations utilizing standard and stabilized versions of the realizable k–ε model are presented in Fig. 5. These results utilize initial conditions $(\eta_0, \gamma_0) = (3.5, 1.09)$ such that they are in the proved "event horizon" region for the standard model. As seen in Fig. 5, with the standard closure model, after some initial development, the eddy viscosity begins to grow exponentially at a rate reasonably in line with (though slightly less than) that predicted by the simplified analysis. This growth continues until the eddy viscosity reaches several thousand times the fluid viscosity, ultimately causing unphysical decay of the wave and destroying the simulation. Alternatively, with the stabilized model, the eddy viscosity quickly decays to insignificant levels, and the wave propagates with nearly constant form. The slight decay seen is due to minor numerical diffusion. This has been

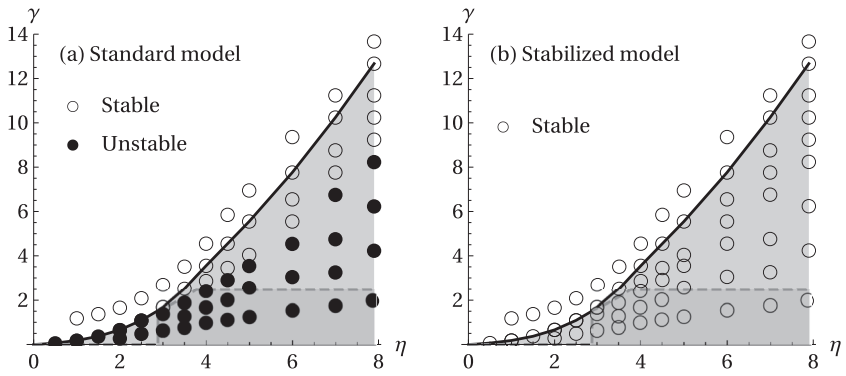

FIG. 4. Summary of CFD simulations using various initial conditions in terms of (η_0, γ_0) with (a) standard and (b) stabilized realizable k–ε turbulence models. The shaded regions depict the unstable range of initial conditions from Fig. 2.

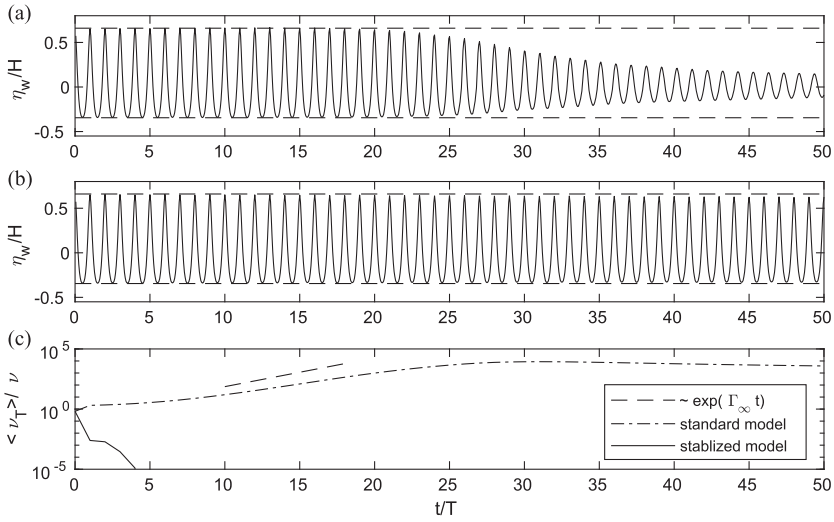

FIG. 5. Computed surface elevation (η_w) time series from progressive wave simulations using (η_0, γ_0) = (3.5, 1.09) with the (a) standard and (b) stabilized (λ_2 = 0.05) realizable k–ε model. The series for the period- and depth-averaged eddy viscosity $\langle \nu_T \rangle$ (both models) is shown in (c).

confirmed by comparison with an otherwise identical simulation but with the turbulence model switched off entirely, which yields visually indistinguishable results for the surface elevation, as depicted in Fig. 5(b).

B. Breaking wave simulations

Having largely confirmed the conditional instability of the realizable k–ε model in the nearly potential flow region beneath non-breaking surface waves, let us now compare simulations involving spilling breaking waves, based on the experimental conditions of Ting and Kirby.[8] The computational domain utilized in these simulations is depicted in Fig. 6. The domain resembles that utilized previously by LF18,[1] except that herein the total length of the computational domain is set as 40 m, matching the length of the experimental wave flume utilized by Ting and Kirby.[8] This case utilizes the same wave specifications as in Subsection IV A, where the waves are generated utilizing a relaxation zone, as depicted in Fig. 6. The initial conditions utilized for the turbulence model correspond to (η_0, γ_0) = (3.5, 0.88), which is again in the proved unstable "event horizon" region for the standard model. The models have been run for a total duration of 120T. The first 60T have been considered as warm up, ensuring full development, whereas the final 60T have been utilized for averaging, when relevant. We will here focus on presenting distinct, qualitative differences between the results utilizing standard and stabilized variations of the realizable k–ε model.

As a first means of qualitative comparison, the computed non-dimensional eddy viscosity ν_T/ν for otherwise identical simulations using standard (λ_2 = 0 such that $\tilde{\varepsilon}$ = ε) and stabilized (λ_2 = 0.05) variations of the model are presented in Fig. 7 at time instant t = 80T. From Fig. 7(a), it is seen that utilizing the turbulence model in its standard form has resulted in the eddy viscosity reaching several hundred times that of the fluid even prior to breaking (incipient breaking occurs at $x \approx 6.4$ m). This is not physical and is a consequence of the instability being triggered in the nearly potential flow region beneath the non-breaking waves, as discussed at length above. Conversely, when utilizing the stabilized model [Fig. 7(b)], there is only significant eddy viscosity (hence turbulence) within the surf zone region, i.e., after the waves have broken, as should be expected on physical grounds. (It is emphasized that the turbulence model is also active in the bottom boundary layer region in both cases, but this region is very thin and difficult to see in Fig. 7).

The qualitative consequences of the above are further demonstrated in Fig. 8, which depicts the computed surface elevation envelopes and mean water levels from both simulations, which are also compared with the experimental measurements (shown as open

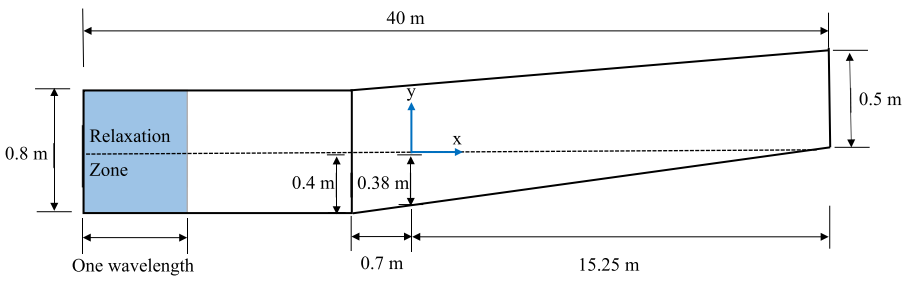

FIG. 6. Sketch of the computational domain used in the (spilling) breaking wave simulations.

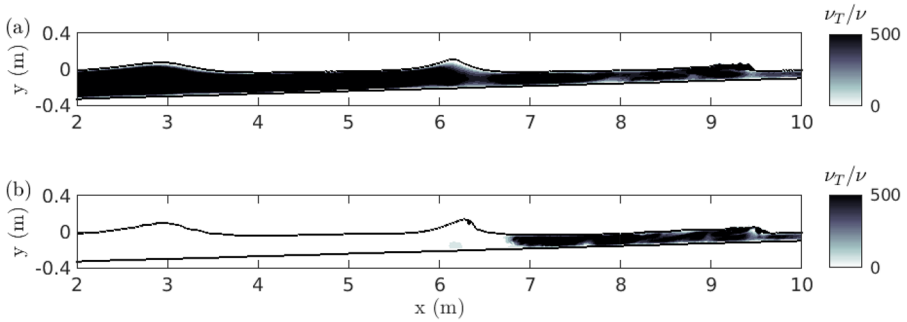

FIG. 7. Computed non-dimensional eddy viscosity (ν_T/ν) at $t = 80T$ for simulations using the (a) standard and (b) stabilized realizable k–ε turbulence closure model.

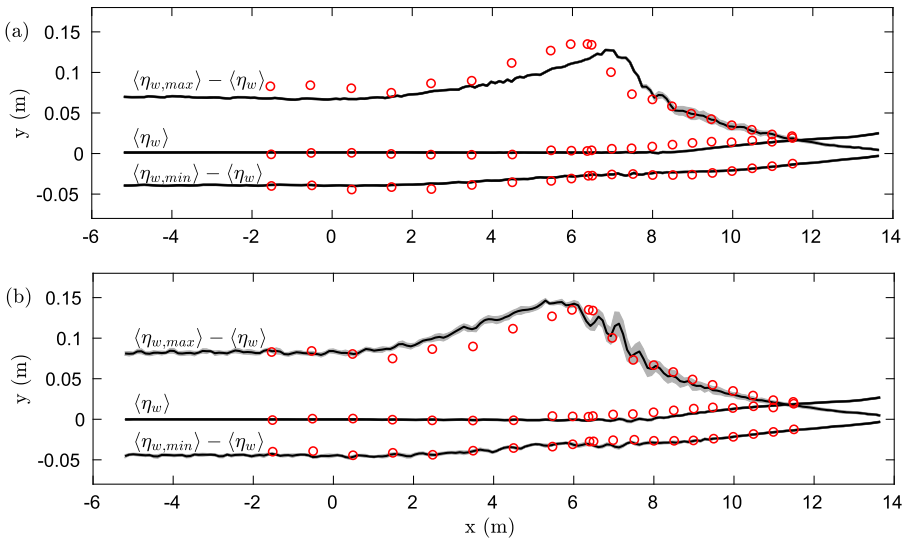

FIG. 8. Computed surface elevation envelopes and mean water levels using the (a) standard and (b) stabilized realizable k–ε turbulence closure models. The shaded gray regions depicts plus/minus one standard deviation.

circles). From Fig. 8(a), it is seen that the unstable growth of turbulence prior to breaking has caused un-physical decay of the waves during the shoaling process, which, in turn, delays the onset of breaking. This is problematic as a turbulence model should not be expected to significantly alter the breaking point. Conversely, the results utilizing the otherwise identical stabilized turbulence closure model are depicted in Fig. 8(b). In this simulation, the turbulence model was essentially only active within the surf zone [see again Fig. 7(b)], resulting in a breaking process that is much closer to that observed experimentally.

More detailed investigations on the differences in the computed undertow velocity and turbulence kinetic energy density profiles have also been made. These follow essentially similar tendencies as have already been shown by LF18[1] (in their case utilizing a k–ω turbulence model) and are hence not shown here for the sake of brevity.

V. CONCLUSIONS

It has been proved that the realizable k–ε turbulence model of Shih *et al.*[5] is conditionally unstable in the nearly potential flow region beneath surface waves, which can result in unphysical exponential growth of the turbulent kinetic energy and eddy viscosity. The range of initial conditions ultimately leading to instability has been systematically investigated. Following the previous methodology presented by Larsen and Fuhrman,[1] a method for formally stabilizing the model has likewise been developed through the addition of a limited form of the ε variable (called $\tilde{\varepsilon}$ within) in the eddy viscosity. Both the conditional instability, and the resulting stabilization, have been confirmed through CFD simulations of surface wave trains and of spilling breaking waves. To avoid potential for unphysical overproduction of turbulence beneath surface waves, it is recommended that formally stabilized versions be utilized whenever this closure is adopted in CFD simulation of surface waves.

ACKNOWLEDGMENTS

D.R.F. acknowledges financial support from the Independent Research Fund Denmark (project SWASH: Simulating WAve Surf-zone Hydrodynamics and sea bed morphology, Grant No. 8022-00137B). Y.L. acknowledges funding from the European Union's Horizon 2020 research and innovation program, Marie Sklodowska-Curie Grant No. 713683 (COFUNDfellowsDTU, H. C. Ørsted Postdoc project SUBSEA: SimUlating Breaking waves and SEdiment trAnsport with stabilized turbulence models).

DATA AVAILABILITY

The data that support the findings of this study are available from the corresponding author upon reasonable request.

REFERENCES

[1]B. E. Larsen and D. R. Fuhrman, "On the over-production of turbulence beneath surface waves in Reynolds-averaged Navier-Stokes models," J. Fluid Mech. **853**, 419–460 (2018).
[2]S. Mayer and P. A. Madsen, "Simulations of breaking waves in the surf zone using a Navier-Stokes solver," in *Proceedings of the 29th International Conference on Coastal Engineering, Sydney, Australia* (American Society of Civil Engineering, 2000), pp. 928–941.
[3]P. Lin and P. L.-F. Liu, "A numerical study of breaking waves in the surf zone," J. Fluid Mech. **359**, 239–264 (1998).
[4]S. A. Brown, D. M. Greaves, V. Magar, and D. C. Conley, "Evaluation of turbulence closure models under spilling and plunging breakers in the surf zone," Coastal Eng. **114**, 177–193 (2016).
[5]T.-H. Shih, W. W. Liou, A. Shabbir, Z. Yang, and J. Zhu, "A new k-ϵ eddy viscosity model for high Reynolds number turbulent flows," Comput. Fluids **24**, 227–238 (1995).
[6]J. D. Fenton, "The numerical solution of steady water wave problems," Comput. Geosci. **14**, 357–368 (1988).
[7]N. G. Jacobsen, D. R. Fuhrman, and J. Fredsøe, "A wave generation toolbox for the open-source CFD library: OpenFoam," Int. J. Numer. Methods Fluids **70**, 1073–1088 (2012).
[8]F. C. K. Ting and J. T. Kirby, "Observation of undertow and turbulence in a laboratory surf zone," Coastal Eng. **24**, 51–80 (1994).